

^3He in the Milky Way Interstellar Medium: Ionization Structure

T. M. Bania¹, Dana S. Balser², Robert T. Rood³, T. L. Wilson⁴, & Jennifer M. LaRocque⁵

ABSTRACT

The cosmic abundance of the ^3He isotope has important implications for many fields of astrophysics. We are using the 8.665 GHz hyperfine transition of $^3\text{He}^+$ to determine the $^3\text{He}/\text{H}$ abundance in Milky Way H II regions and planetary nebulae. This is one in a series of papers in which we discuss issues involved in deriving accurate $^3\text{He}/\text{H}$ abundance ratios from the available measurements. Here we describe the ionization correction we use to convert the $^3\text{He}^+/\text{H}^+$ abundance, y_3^+ , to the $^3\text{He}/\text{H}$ abundance, y_3 . In principle the nebular ionization structure can significantly influence the y_3 derived for individual sources. We find that in general there is insufficient information available to make a detailed ionization correction. Here we make a simple correction and assess its validity. The correction is based on radio recombination line measurements of H^+ and $^4\text{He}^+$, together with simple core-halo source models. We use these models to establish criteria that allow us to identify sources that can be accurately corrected for ionization and those that cannot. We argue that this effect cannot be very large for most of the sources in our observational sample. For a wide range of models of nebular ionization structure we find that the ionization correction factor varies from 1 to 1.8. Although larger corrections are possible, there would have to be a conspiracy between the density and ionization structure for us to underestimate the ionization correction by a substantial amount.

Subject headings: H II regions — ISM: abundances — radio lines: ISM

¹Institute for Astrophysical Research, Department of Astronomy, Boston University, 725 Commonwealth Avenue, Boston MA 02215, USA. (bania@bu.edu)

²National Radio Astronomy Observatory, 520 Edgemont Rd., Charlottesville, VA 22903, USA.

³P.O. Box 400325, Astronomy Department, University of Virginia, Charlottesville VA 22904-4325, USA.

⁴ESO Room 422, Karl-Schwarzschild-Str. 2, 85748 Garching, Germany

⁵Saint Michael's College, Colchester VT 05439

1. INTRODUCTION

1.1. The ^3He Experiment

The abundance of the light isotope of helium, ^3He , is astrophysically important. Knowing the $^3\text{He}/\text{H}$ abundance ratio can be used to test the theory of stellar nucleosynthesis; it gives important information needed to evaluate models of Galactic chemical evolution; it can help constrain Big Bang Nucleosynthesis. For over two decades we have used the 8.665 GHz hyperfine transition of $^3\text{He}^+$ to derive the $^3\text{He}/\text{H}$ abundance in the interstellar medium (ISM) of the Milky Way. Our ^3He sources, planetary nebulae and H II regions, are distributed throughout the Milky Way’s disk, from the Galactic Center to the outermost regions. There is no other ^3He spectral transition available that can be used to probe transgalactic paths with the sensitivity and accuracy of the $^3\text{He}^+$ hyperfine line.

We observed $^3\text{He}^+$ using the Max-Planck-Institut für Radioastronomie (MPIfR) 100 m telescope and the National Radio Astronomy Observatory (NRAO)¹ 140 Foot telescope and Very Large Array (VLA). With the 100 m and VLA we primarily studied planetary nebulae (Balsler et al. 1997, 2006) whereas the 140 Foot was used mostly for H II regions (Bania et al. 1997, hereafter Paper I). In addition to the $^3\text{He}^+$ observations, measurements were also made of a variety of radio recombination line transitions (RRLs) of H, ^4He , and C, as well as of the thermal continuum emission from the nebulae. Paper I discussed the observations and the measurement errors. It is a summary of the status of the observations as of 1996 March. We continued the $^3\text{He}^+$ program on the 140 Foot until it was decommissioned in 1999 July. (The last scientific spectrum observed at the 140 Foot telescope was the $^3\text{He}^+$ scan that finished at 08:12:20 EDT 19 July 1999.) The final paper in this series (Rood et al. 2007, Paper IV) summarizes the results of the $^3\text{He}^+$ experiment for all the sources observed with the NRAO 140 Foot telescope during the period 1982–1999. Paper IV compiles the observed properties of the $^3\text{He}^+$ emission and gives the final $^3\text{He}/\text{H}$ abundances derived for the NRAO 140 Foot sample of $^3\text{He}^+$ H II regions.

The quantity of astrophysical interest is the $^3\text{He}/\text{H}$ abundance ratio by number which we define as y_3 . This ratio provides information about both stellar (Charbonnel 1998) and Galactic chemical evolution (Romano et al. 2003) and constrains cosmological models during the era of primordial nucleosynthesis (Yang et al. 1984; Bania et al. 2002). The species directly accessible to observation, however, are $^3\text{He}^+$ and H^+ . The collisionally excited $^3\text{He}^+$ hyperfine transition directly measures the total column density of $^3\text{He}^+$ atoms along the

¹The National Radio Astronomy Observatory is a facility of the National Science Foundation operated under cooperative agreement by Associated Universities, Inc.

line-of-sight within the telescope’s beam. To determine the column density of H^+ , either radio continuum or hydrogen RRLs can be used. At 8.7 GHz the radio continuum emission in H II regions and planetary nebulae is primarily due to thermal free-free emission which is proportional to the emission measure, $EM = \int n_e^2 dl$, where n_e is the electron density and dl is the differential path length through the ionized nebula. The H RRL emission is also proportional to the emission measure. Thus neither the RRL nor the radio continuum data for H^+ are probing the total proton column density (or mass) in a straightforward manner. *In order to determine the $^3\text{He}^+/\text{H}^+$ abundance ratio, it is therefore necessary to model the nebula’s density structure.* Models are required because in most cases detailed information on nebular density structure is not observationally accessible. Nebular density models and the $^3\text{He}^+/\text{H}^+$ abundance ratios derived from them are discussed by Balser et al. (1999, hereafter Paper II). In particular, Table 5 of Paper II lists the adopted $^3\text{He}^+/\text{H}^+$ abundance ratios for the 21 H II regions discussed in Paper I.

Using the observables, $^3\text{He}^+$ and H^+ , to derive a $^3\text{He}/\text{H}$ abundance ratio, y_3 , is, however, a two step process. The first step is to determine the source density structure and calculate $^3\text{He}^+/\text{H}^+$ (Paper II). The next step, the topic of this paper, is to determine the source ionization structure and to use this information to convert $^3\text{He}^+/\text{H}^+$ into $^3\text{He}/\text{H}$. This requires an understanding of the ionization properties of each ionized nebula. Specifically, one needs to know the ionization structure of both the He and H throughout each nebula. Because the first ionization potentials of H (13.6 eV) and He (24.6 eV) are nearly a factor of two different, in principle ionization can significantly influence y_3 for individual sources. We find that in general there is insufficient information available to make a detailed ionization correction. Here we make a simple correction and assess its validity.

1.2. Helium Ionization Structure in H II Regions

Several diagnostics are commonly used to study the helium ionization structure in H II regions. The most direct is to measure the fraction of $^4\text{He}^0$, $^4\text{He}^+$, and $^4\text{He}^{++}$ within the H II (H^+) region. Since both ^4He and ^3He have essentially the same ionization potential the $^3\text{He}^+$ and $^4\text{He}^+$ emission should come from identical zones within the nebula. The $^4\text{He}^+$ and $^4\text{He}^{++}$ emission can be measured using recombination lines. Unfortunately there is no direct way of measuring the amount of neutral helium within the H II region. In some cases the spectral types of the ionizing OB stars can be identified from optical photometry and spectroscopy. The helium ionization properties are then derived using stellar atmosphere models to calculate the expected escaping flux (e.g., Vacca et al. 1996), together with photoionization models of the nebula to determine the He ionization structure (e.g., Rubin 1984). At optical wave-

lengths spectral transitions of several other atomic species are also observed to help constrain these models. The most detailed analyzes have been made for the Orion nebula in order to determine the total $^4\text{He}/\text{H}$ abundance ratio (Mathis & Rose 1991; Baldwin et al. 1991; Rubin et al. 1991; Pogge et al. 1992; Esteban et al. 1998; Blagrove et al. 2007). Nevertheless, the limiting factor in determining accurate total helium abundances in Orion is in converting $^4\text{He}^+/\text{H}^+$ to $^4\text{He}/\text{H}$.

Most H II regions are ionized by several stars and may thus have a complex geometry. Because of this little direct information may be known about the radiation field. A variety of diagnostics have been developed to probe the ionization structure. Vílchez & Pagel (1988) developed a radiation softness parameter based on the fine structure lines of O and S ions that is not very sensitive to chemical composition (see also Shields & Searle 1978; Mathis 1982, 1985). Armour et al. (1999) use infrared transitions of Ne and Ar ions to determine the ionization structure. In general H II regions ionized by a hard radiation field produce the most accurate $^4\text{He}/\text{H}$ abundance ratios since all of the helium within the H II regions will be ionized. For example, metal poor blue compact galaxies with H II regions ionized by hard radiation fields are used to measure primordial $^4\text{He}/\text{H}$. The ionization structure of these objects has been extensively studied (Ballantyne et al. 2000; Viegas et al. 2000; Gruenwald et al. 2002; Sauer & Jedamzik 2002; Peimbert et al. 2002; Izotov et al. 2007). In some cases the total $^4\text{He}/\text{H}$ abundance ratio will be less than $^4\text{He}^+/\text{H}^+$ by a few percent, significant for cosmological implications, since the He II zone is larger than the H II zone. If clumping exists in these H II regions, however, the determined y_4 values will be underestimated by a few percent (Mathis & Wood 2005). In the Galaxy the high excitation H II regions M17 and S206 have been used instead of Orion to determine the total $^4\text{He}/\text{H}$ abundance ratio (Peimbert 1993; Esteban et al. 1999; Deharveng et al. 2000; Balser 2006).

Many of our sources are located throughout the Galactic disk and are totally obscured at optical wavelengths by dust. Furthermore, most of the optically visible H II regions in our sample are low emission measure H II regions in the outer Galaxy. The low EM renders useless the Orion-type detailed models since the spectral diagnostics used to constrain them are not available. Fortunately, unlike many of the light elements, $^3\text{He}/\text{H}$ abundances accurate to $\sim 10\%$ can yield important astrophysical conclusions (Wilson & Rood 1994). Because of this we adopt here a simple ionization structure model that is constrained primarily by H and ^4He radio recombination line observations. We then use numerical models to assess the accuracy of this approach for the H II regions in our sample. Our goal is to identify a subset of sources in our nebular sample wherein we can derive $^3\text{He}/\text{H}$ abundances accurate to $\sim 10\%$.

1.3. ^3He Ionization Correction

We seek an ionization correction factor to derive the $^3\text{He}/\text{H}$ abundance from the $^3\text{He}^+/\text{H}^+$ abundance gotten from the $^3\text{He}^+$ observations. We define the ionization correction factor, κ_i , to be $y_3 \equiv \kappa_i y_3^+$, where y is the He/H abundance ratio by number, the subscript denotes the isotope, and the superscript is the ionization state.² The ionization correction factor is determined by using the H and ^4He radio recombination line observations. We assume that the $^3\text{He}^+$ emission traces the $^4\text{He}^+$ emission, that the amount of neutral and doubly ionized helium is negligible, and a canonical value for the total $^4\text{He}/\text{H}$ abundance, y_4 . The $^3\text{He}/\text{H}$ abundance ratio is then given by

$$y_3 = \left(\frac{y_4}{y_4^+}\right) y_3^+ = \kappa_i y_3^+ \left(\frac{y_{4\text{GAL}}}{0.10}\right). \quad (1)$$

Here $y_{4\text{GAL}}$ is the actual $^4\text{He}/\text{H}$ abundance by number in the Milky Way. There are, of course, some problems with this simple model. $^3\text{He}^+$ and $^4\text{He}^+$ are measured using transitions that are sensitive in different ways to density structure within the nebula. The $^3\text{He}^+$ is observed using a collisionally excited hyperfine transition that is sensitive to the column density and thus proportional to the electron density, n_e . The $^4\text{He}^+$ is observed using recombination transitions that are proportional to the emission measure or n_e^2 . Thus if the H II region has large density fluctuations the different transitions may probe significantly different material. For example, consider a simple two-component nebula with a small, very dense core and a larger, diffuse halo. Under certain physical conditions the halo will dominate the $^3\text{He}^+$ emission while the core will dominate the $^4\text{He}^+$ emission. If this is coupled with ionization structure between the core and halo then the simple formula in equation (1) will be incorrect.

It has also proven difficult to measure accurately the $^4\text{He}/\text{H}$ abundance, y_4 , in the Galaxy. ^4He cannot be directly measured in the Sun and must be inferred from theoretical stellar evolution models and helioseismology. Measurements of ^4He in H II regions using recombination lines require an ionization correction as discussed above. A canonical value of $y_4 = y_{4\text{GAL}} = 0.1$ is adopted here although there is evidence that this often cited value may be too high (see §5). For this reason we have parameterized equation (1) with the $y_{4\text{GAL}}$ factor so that our ionization corrections can be easily scaled should an accurate Milky Way y_4 value be derived in the future.

²Thus the notation used throughout is: $y_3 = ^3\text{He}/\text{H}$; $y_3^+ = ^3\text{He}^+/\text{H}^+$; $y_4 = ^4\text{He}/\text{H}$; and $y_4^+ = ^4\text{He}^+/\text{H}^+$.

1.4. Radio Recombination Line Observations

Here we use high signal-to-noise ratio recombination line spectra taken at two different spatial resolutions to probe for any significant ionization structure. For our H II region sample we have obtained H and ^4He RRL data simultaneously for several different transitions near 8 GHz with a spatial resolution of $3'.5$ (see Paper I). These observations are briefly reviewed here in §2.1. Because they sample the same H II region zone as the $^3\text{He}^+$ spectra, these data are primarily used to determine y_4^+ in equation (1). Most ^4He RRL data are from single-dish telescopes which typically have spatial resolutions $\gtrsim 1'$. Measuring accurate y_4^+ abundance ratios with single-dish telescopes is difficult because non-random frequency structure is produced in the instrumental baselines owing to reflections from various parts of the telescope structure (see Lockman & Brown 1982). Improvements in receiver technology have provided better stability and enhanced signal-to-noise. This, together with a better understanding of the instrumental effects, has enabled more accurate measurements of y_4^+ (Peimbert et al. 1992a; Paper I).

Using these improved techniques we made additional observations at 18 GHz with a spatial resolution of $1'.5$ for a subset of our H II region sample (§2.2). The smaller beam of the 18 GHz RRLs typically probes the more compact, dense components, whereas the larger $3'.5$ beam of the 8 GHz RRLs is more sensitive to the extended, diffuse material. Radio interferometers can measure the $^4\text{He}^+$ distribution within H II regions at spatial resolutions $\lesssim 1'$. Although interferometers do not detect the diffuse emission because of the zero-spacing flux problem, this information can be provided by single-dish measurements. To our knowledge only five H II regions in our sample have been observed in H and ^4He RRL emission with radio interferometers: W3, Sgr B2, W43, W49, and W51.

Since the entire nebula can be imaged, the best optical data for this study are observations made with Fabry-Perot spectrophotometers. Caplan et al. (2000) derived oxygen and helium abundances for 34 H II regions using the ESOP Fabry-Perot instrument. For many objects the entire nebula was probed (the largest diaphragm was $4' 27''$). The ^4He abundances from this survey are discussed by Deharveng et al. (2000). There are four H II regions that are in our sample: S206, S209, S212, and S252.

Although the 8 GHz RRLs are primarily used to determine y_4^+ the other radio and optical $^4\text{He}^+$ data can not only provide an independent confirmation of the $^4\text{He}^+/\text{H}^+$ abundance, but also indicate whether the assumptions in equation (1) are valid. In §3 numerical models are used to explore the physical conditions under which the assumptions in equation (1) begin to fail. This information is then used in §4 to determine a value for the ionization correction factor, κ_i , for each source. A discussion of the results is in §5 and a summary of the paper in §6.

2. ${}^4\text{He}^+$ OBSERVATIONS

2.1. X-band (8 GHz) Radio Recombination Lines

The X-band RRL observations are discussed in §2 of Paper I. The $\text{H}91\alpha$ and $\text{He}91\alpha$ transitions were observed in every H II region. Additional, higher order, transitions were also observed at nearby frequencies with essentially the same spatial resolution (3'5). These data were used to constrain the nebular models in Paper II. Here we only use the higher quality 91α and 114β transitions of H and ${}^4\text{He}$.

Calibration details are discussed in §2.1 of Paper I. We used the planetary nebula NGC 7027 to calibrate the flux density scale for each observing epoch. The absolute calibration is judged to be within $\sim 10\%$; the internal consistency is $\sim 5\%$. From these observations we use only the ratios of the line areas to calculate ${}^4\text{He}^+/\text{H}^+$; the calibration is therefore not a significant source of uncertainty.

A much larger source of uncertainty are the standing waves produced by reflections from various parts of the telescope structure (see §2.2 in Paper I and references therein). To minimize the amplitude of these standing waves, observations are made with focus offsets alternating between $\pm\lambda_0/8$ every 60 s. Cancellation of the standing waves is, however, not perfect and the spectral baselines must be modeled. A 12th order polynomial baseline is used to model this non-random frequency structure. The necessity for using a high-order baseline and the selection of the appropriate order to be used is discussed in Balser et al. (1994) and Paper I. The results of Gaussian fits to each transition are given in Table 4 of Paper I.

2.2. K-band (18 GHz) Radio Recombination Lines

Observations of H and ${}^4\text{He}$ RRLs at K-band were made with the NRAO 140 Foot telescope during the periods: 1995 November, 1995 December, and 1996 January. The 140 Foot telescope has a half-power beam-width of 1'5 at 18 GHz. The radiometer consisted of a dual circularly polarized HEMT receiver located at the Cassegrain focus of the 140 Foot telescope. The system temperature on cold sky under good weather conditions was ~ 50 K. The spectrometer consisted of the NRAO model IV 1024 channel autocorrelator (AC). The AC sampled four independent 20 MHz wide frequency bands (“quadrants”) of 256 channels each. The velocity resolution at 18 GHz is 1.3 km sec^{-1} . The 20 MHz bandwidth allowed both the H and ${}^4\text{He}$ transitions to be observed simultaneously within each quadrant. For most of the observing the AC was configured with the $\text{H}70\alpha/\text{He}70\alpha$ and the $\text{H}88\beta/\text{He}88\beta$ RRLs in two quadrants each, simultaneously sampling orthogonal polarizations in order to maximize

our spectral sensitivity. In some of the brighter objects the 100γ and 110δ transitions of H and ^4He were observed.

Spectra were taken using the total power observing mode. First a reference spectrum (OFF) was taken at a position offset 6 minutes in right ascension from the nebula and then the nebula itself (ON) was observed. Each position had an integration time of 6 minutes. Local pointing corrections were determined every hour. After each pointing a continuum cross scan, in right ascension and declination, was made on the H II region to measure the radio continuum emission.

The radiometer system temperature was measured using noise tubes calibrated by connecting the receiver to matched hot and cold loads. An ambient temperature absorber was used for the hot load and the zenith sky for the cold load. Since this procedure has many uncertainties and is not always performed before each observing session we have re-calibrated the system temperature by using the observed continuum intensity of the unresolved planetary nebula NGC 7027. NGC 7027 was observed several times during each observing session during good weather near transit; it has a flux density of 6 Jy at 18 GHz (Peng et al. 2000).

There are two effects that can modify the calibration as a function of time. First, at these frequencies the aperture efficiency of the 140 Foot telescope changes with elevation as gravity distorts the primary reflector; an elevation gain correction must therefore be made. We measured the H II region continuum intensity every hour for each source in order to determine the appropriate gain correction. Second, the atmospheric opacity is significant and depends on the water vapor content. We made a tipping scan several times during each observing period to measure the opacity. Since we are interested in calculating the $^4\text{He}^+/\text{H}^+$ abundance ratio, which depends on the ratio of the line intensities, the calibration effectively cancels. All intensities quoted here are therefore antenna temperatures calibrated using only the NGC 7027 data.

We used the techniques discussed in §2.2 of Paper I to model the K-band spectral baselines, except that a 6th order polynomial was used instead of a 12th order. Although the AC configuration was the same, yielding a 20 MHz bandwidth with 256 channels, only ~ 12 MHz is required to cover the frequency range between the H and ^4He lines. We have therefore reduced the total number of terms in the polynomial baseline model.

2.3. The $^4\text{He}^+/\text{H}^+$ Abundance Ratio

Example RRL spectra are shown in Figure 1. Only 10 objects from the original sample of 21 were observed at K-band. The data were smoothed to a velocity resolution of 8.1 km sec^{-1} .

The vertical lines flag the expected locations of the H, He, and C lines for the specified RRL transition (91α or 70α). Table 1 summarizes the results of Gaussian fits to the K-band spectra. Listed are the source name, the RRL transition, the peak intensity and full-width half-maximum (FWHM) line-width together with their associated errors, the total integration time, the resulting r.m.s. noise of the spectral baseline, and the quality factor of the line. The quality factor is determined using the same criteria as in Paper I. These include the signal-to-noise ratio, the structure of the baseline, and the crowding of spectral lines. We do not include any calibration error in assessing the quality factor since we only use line ratios in this paper.

The ${}^4\text{He}^+/\text{H}^+$, y_4^+ , abundance ratios calculated from the RRL data using the line areas are summarized in Figure 2 which plots the y_4^+ abundance ratio as a function of the principal quantum number, n , of the RRL transition. The 70α , 88β , 91α , and 114β transitions are shown. The Gaussian line parameters in Table 4 of Paper I and in Table 1 here are used for the X-band and K-band transitions, respectively. The errors are determined by propagating the uncertainties in the Gaussian fit to the line intensity and width.

For some nebulae there are real differences among the y_4^+ ratios derived from the various RRL transitions. This is to be expected, of course, since the K-band spectra probe, on average, the denser, more compact nebular interior whereas the X-band spectra measure a much larger region, perhaps including a low density halo. These statistically significant differences are clearly seen in Figure 3 which compares in various ways the y_4^+ ratios derived from the H91 α (diamonds) and H70 α (circles) spectra for the 10 K-band sources (see §5).

3. SYNTHETIC NEBULAR MODELS

We use the formalism defined in §1.3 together with numerical models for the nebulae to explore the range of validity of this approach to the ionization correction. The H II regions in our sample span a wide range of physical conditions. At one extreme there are large, complex H II regions such as W49 that are ionized by many OB-type stars and have multiple compact components in their density structure. At the other extreme are H II regions such as S206, which are smaller, much less complex sources, that are probably ionized by a single OB-type star. The simple ionization structure correction model discussed in §1.3 could well not be very accurate for sources like W49. It is important, however, to understand under what conditions this model breaks down and what impact this has on deriving ${}^3\text{He}/\text{H}$ abundance ratios.

Paper II explored the effect of source density structure on the derivation of the ${}^3\text{He}/\text{H}$

abundance. We used RRL and continuum data to constrain the models. Both RRL and continuum emission intensities are proportional to n_e^2 and so they trace the densest components of the nebulae. We found that our sources could be grouped into two broad categories. In one class were “complex,” W49-like sources that required models with complex density structure and non-LTE radiative transfer in order to reproduce the observations. In the other class were “simple,” S206-like sources whose observations could be reproduced by models with LTE radiative transfer and homogeneous density structure.

We adopt a simple core-halo model for the nebular density and ionization structure. From the models we calculate simulated observations and assess the effect of the model structure on our ability to recover accurately the $^3\text{He}/\text{H}$ abundance using our simple ionization structure correction. We use a computer program called NEBULA to model the H II region (see Balser 1995 and Paper II for details about NEBULA). The model nebula can have arbitrary density, temperature, and ionization structure. The gas consists of only hydrogen and helium. We calculate the radiative transfer through the model nebula for the radio continuum, recombination line, and $^3\text{He}^+$ hyperfine line emission. Since we shall be comparing these synthetic spectral lines to the §2 data taken at 8 and 18 GHz, we calculate the model antenna temperature for each species by convolving the model sky brightness temperature distribution with the telescope beam and multiplying by the telescope main beam efficiency. The telescope beam is assumed to be a Gaussian with a half-power beam-width (HPBW) of 1'5 or 3'5. These are the HPBW sizes of the 140 Foot telescope beam at 18 GHz and 8 GHz, respectively.

All model nebulae are located at a distance of 8 kpc which is roughly the average distance to our ^3He sources. The models are comprised of nested, spherical, homogeneous, isothermal components. For simplicity, all model components have a fixed, 8,000 K, electron temperature that is typical for Galactic H II regions. For all models it is assumed that the total abundance ratios are $y_3 \equiv 1 \times 10^{-5}$ and $y_4 \equiv 0.10$. Table 2 summarizes the model parameters used as input for the NEBULA program.

Model A is a one-component, low density, $n_e = 100 \text{ cm}^{-3}$, nebula with an angular size of 3'5 (8.14 pc). All other models are two-component (core-halo) nebulae which consist of a 1'5 (3.49 pc) core embedded in a larger 3'5 nebula. Listed for each component is the angular size, the electron density, the fraction of the component H II mass relative to the total mass, the y_3^+ abundance ratio, and the y_4^+ abundance ratio. Altogether, the models span a core-halo density contrast ratio from 1:1 to 5:1, and a core mass fraction from 8% to 30%. That is, all models have halos that contain more mass than the cores by a factor of either ~ 2 or ~ 10 . These parameters span the range of the Galactic H II region physical properties derived from single-dish RRL observations (e.g., Quireza et al. 2006a,b).

The NEBULA code calculates the following observable quantities: the continuum antenna temperature at 8.665 GHz and the antenna temperatures of the $^3\text{He}^+$, H91 α , He91 α , H70 α , and He70 α transitions. Properties of the synthetic observations that result from the Table 2 models are summarized in Table 3. Listed are the continuum and line antenna temperature for the $^3\text{He}^+$ transition, the y_3^+ ($^3\text{He}^+/\text{H}^+$) abundance ratio, the y_4^+ ($^4\text{He}^+/\text{H}^+$) abundance ratio and the values of κ_i and y_3 calculated using the equation (1) Ansatz. All of these quantities are determined for X-band (8 GHz). The last column lists the y_4^+ model values at K-band (18 GHz). The y_4^+ values are calculated from the H and ^4He line parameters produced by NEBULA; they are the ratio of the line areas. The y_3^+ value is derived from the NEBULA models assuming a single, homogeneous, fully ionized sphere where $y_3^+ \propto T_L \Delta v / T_C^{1/2}$. This analytical expression approximates the numerical calculation to within a few percent (see Balser 1995). This is our standard way of deriving the $^3\text{He}/\text{H}$ abundance ratio (Paper II). Here we apply this analysis to the Table 2 nebular models and use the formalism developed in §1.3 to derive the ionization correction factor, κ_i .

Model A1 is a uniform nebula with no density or ionization structure. The NEBULA model abundances in Table 3, y_3^+ and y_4^+ , exactly match the input abundances, $y_3 = 1 \times 10^{-5}$ and $y_4 = 0.10$. This of course must be the case since Model A1 is constructed to match our analysis assumptions. It is a single, homogeneous, fully ionized sphere and the NEBULA Model A1 gives an ionization correction of $\kappa_i = 1$ as it should.

In Model A2 we simulate a one-component nebula that has 30% of all the helium neutral. For this model the NEBULA ^4He RRL synthetic spectra together with equation (1) give an ionization correction of $\kappa_i = 1.4$ which in turn produces $y_3 = 1.0 \times 10^{-5}$, the model input abundance. Thus, for a one-component model nebula the observables are sufficient to derive ionization corrections that can accurately recover the input structure.

Model B has a core-halo density structure where the core component has a higher density by a factor of 5, but the halo has a factor of ~ 2.3 times more mass. Both core and halo are fully ionized: Model B has no ionization structure so we cannot derive any correction factor. The NEBULA Model B y_3^+ abundance thus underestimates the true y_3^+ abundance by a factor of 1.3. In Paper II we discuss density structure corrections for the $^3\text{He}^+/\text{H}^+$ abundance ratio derivation. There we model nebular density structure and estimate the density correction factor for each H II region in our sample. Applying these techniques to Model B recovers, as expected, the input y_3^+ abundance.

Models C and D are constant density nebulae with core-halo ionization structure. The halo mass in both models is ~ 11.5 times that of the core. Model C has a fully ionized core and a halo that is under-ionized by 50%. Model D reverses this ionization structure. That these models have ionization structure is revealed by the different NEBULA values for the X

and K-band y_4^+ abundance ratios (see Table 3). Since most of the mass resides in these halos the NEBULA ${}^3\text{He}^+/\text{H}^+$ abundance ratio is much less for Model C with its under-ionized halo ($y_3^+ = 0.57$) than for model D ($y_3^+ = 0.96$). The NEBULA results give ionization corrections of $\kappa_i = 1.82$ and 1.05 for models C and D, respectively. In both cases Equation 1 yields $y_3 = 1.0 \times 10^{-5}$, the model input value. For these two models our simple ionization correction reproduces the correct ${}^3\text{He}/\text{H}$ abundance ratio.

Models E and F combine both density and ionization structure in a core/halo geometry. Both have high density cores (5:1 density contrast) and halo masses that are ~ 2.3 times that of the cores. Model E has a fully ionized core and a halo that is under-ionized by 50%. Model F reverses this ionization structure. Once again the different NEBULA values for the X and K-band y_4^+ abundance ratios reveal the presence of nebular ionization structure. For model E the NEBULA y_3^+ value is 0.53, roughly a factor of two too low. Yet the NEBULA y_4^+ abundance ratio implies only a small ionization correction factor, $\kappa_i = 1.18$, which gives a corrected y_3 abundance of only 6.2×10^{-6} , 62% of the input value. The situation is much better for Model F with its fully ionized halo. The NEBULA values for y_4^+ and y_3^+ together give an ionization correction factor of $\kappa_i = 1.56$ and a y_3 abundance that is within 2% of the input value.

These models show that the simple ionization correction given in Equation 1 will be reasonably accurate for nebulae with core/halo geometries. Our correction begins to break down whenever the low density component contains most of the mass and is under-ionized. This is because the ${}^3\text{He}^+$ and RRL emission arises from gas located in different zones of the nebula and these regions do not have the same He ionization structure.

In sum, the simple ionization correction given by equation (1) provides a reasonable value for the total y_3 abundance ratio except for the Model E H II region that has an under-ionized halo containing a significant fraction of the total mass. Clearly more complicated density and ionization structures exist in real H II regions. The simple models discussed here nevertheless illustrate the main issues. The simple ionization correction breaks down when ionization structure exists between significantly different density components. True variations of y_4 and y_3 structure within the H II region will complicate the analysis. Nonetheless, because of our large X-band beam that in many cases covers the entire nebula, emission from dense, compact components tends to be diluted. We thus derive an average value of y_3 for each object.

4. IONIZATION CORRECTION FACTOR

Here we assess the ionization structure correction for our ${}^3\text{He}$ sample of 21 Galactic H II regions. In Paper II we classify nebulae into two categories: (i) “simple” H II regions dominated by low-density, extended structure that is well fit by a single-component uniform density sphere model; and (ii) “complex” H II regions that have multiple high density components and thus require a more sophisticated model. The simple H II regions are: G133.8, S206, S209, S212, S228, S235, S252, S311, S76, S90, S156, NGC 7538, and S162; the complex H II regions are: W3, Sgr B2, G1.1, M17S, M17N, W43, W49, and W51. Simple H II regions characteristically have low emission measure. For complex H II regions that have significant ionization structure we will underestimate κ_i as discussed in §3. We therefore can only derive a lower limit to the ${}^3\text{He}/\text{H}$ abundance for these nebulae.

We used various techniques to assess the excitation state of the nebulae. Table 4 summarizes the excitation properties for our H II region sample. Listed for the radio data are the ${}^4\text{He}^+/\text{H}^+$ abundance ratio, y_4^+ , derived using only the H91 α and He91 α RRLs, the H-ionizing luminosity, N_L , determined from the radio continuum data in Paper I, and the spectral type of a single ZAMS star that can produce the observed luminosity. Spectral types are derived from stellar atmosphere models: both the Vacca et al. (1996) and Panagia (1973, in parentheses) models are listed. Similar results from optical data are taken from the literature. The spectral types are based on photometry and spectroscopy; the earliest type star thought to ionize each nebula is listed in Table 4. Overall, the radio and optical spectral classifications are in good agreement.

We plot the ionization state, y_4^+ , of the 14 nebulae for which we have sufficient information as a function of the log of the H-ionizing luminosity, N_L , in Figure 4. There is no discernible trend connecting y_4^+ and N_L . Except for their systematically lower N_L values (recall they are low emission measure nebulae), the simple sources span the same y_4^+ range as do the complex nebulae. Values of N_L determined from the radio continuum include the contribution of H-ionizing photons from all of the early-type stars within the H II region complex. Therefore low emission measure does not necessarily imply that the radiation field is soft. For example the radiation field of the low emission measure Rosette nebula is dominated by O4 stars compared to the rather weak ionization field of the high emission measure Orion nebula.

Below we discuss each H II region separately in more detail. An ionization correction factor, κ_i , is determined for each object. For consistency we only use data as of 1996 March (cf., Papers I and II). The κ_i values can be multiplied by the ${}^3\text{He}^+/\text{H}^+$ abundance ratios in Table 5 of Paper II to yield the ${}^3\text{He}/\text{H}$ abundance. Rood et al. (2007) derive ${}^3\text{He}/\text{H}$ abundances for all the ${}^3\text{He}$ nebulae using the entire 1982–1999 140 Foot dataset.

W3 — Although W3 is optically obscured it has been extensively studied at radio wavelengths. Our higher spatial resolution K-band data give $y_4^+ = 0.081$ whereas the X-band data yield $y_4^+ = 0.076$. Both data sets are of very high quality. One interpretation of these results is that the more compact components of W3—in particular W3A—have a higher excitation than the outer regions probed by the larger X-band beam. This is sometimes called the geometric effect where y_4^+ ratios increase with higher resolution observations.

Interferometers can probe the RRL emission of the nebular gas at high spatial resolution. Extant observations include: 76α and 110α data from the Very Large Array (VLA) and the Westerbork Synthesis Radio Telescope (WSRT) (Roelfsema & Goss 1991) and 92α from the VLA (Roelfsema et al. 1992; Adler et al. 1996). The ${}^4\text{He}^+/\text{H}^+$ abundance ratio varies considerably among the different components ($0.06 \leq y_4^+ \leq 0.20$). Values of y_4^+ higher than 0.10 are thought to be due to local enrichment from a nearby evolved object. Alternatively, radiative transfer effects may cause one to overestimate the true y_4 abundance (Gulyaev et al. 1997). High y_4^+ values in other H II regions are associated with evolved early-type objects (e.g., Balser et al. 2001). W3 is rather unusual in our sample since the total mass of ionized gas is small ($20 M_\odot$; paper I) and therefore mass loss from local objects can significantly pollute the surrounding material. We nevertheless adopt $y_4^+ = 0.076$ as a reasonable value for most of the mass in W3. Because W3 has complex density structure and there is uncertainty about the ionization structure, we adopt an ionization correction of $\kappa_i \geq 1.32$.

G133.8 — Also known as W3N, G133.8 is the northern most region of the W3/W4 complex and has a slightly more negative velocity (by 7 km sec^{-1}) than the other components of W3. Infrared and radio continuum observations of G133.8 indicate that this region is ionized by a luminosity equivalent to an O7 star (Table 4; Schraml & Mezger 1969; Thronson et al. 1984; Carpenter et al. 2000). The X-band RRLs measure $y_4^+ = 0.082$, roughly consistent with the ionization properties predicted from the continuum observations. We adopt an ionization correction of $\kappa_i = 1.22$.

S206 — This outer Galaxy H II region is thought to be ionized by a single star with spectral type O4–O6. Fabry-Perot spectrophotometer data show that S206 contains essentially no neutral helium with $y_4^+ = 0.10$ (Deharveng et al. 2000). Our X-band measurements give a slightly lower value of $y_4^+ = 0.092$. Recent high sensitivity RRL data with the Green Bank Telescope yield $y_4^+ = 0.085$ (Balser 2006). Since we are correcting 140 Foot ${}^3\text{He}$ data, however, we adopt $\kappa_i = 1.09$.

S209 — This H II region has the largest Galactocentric distance, $R_{\text{gal}} = 16.9 \text{ kpc}$, in our entire sample and thus is an important object. Spectrophotometry reveals an O9 and two B1 stars exciting S209 (Chini & Wink 1984); this suggests that S209 might contain some neutral helium. Optical ${}^4\text{He}$ observations show that y_4^+ ranges from 0.084 (Vílchez & Esteban 1996)

to 0.12 (Deharveng et al. 2000). The He91 α transition gives $y_4^+ = 0.083$. We adopt $y_4^+ = 0.083$ producing an ionization correction of $\kappa_i = 1.20$.

S212 — $^3\text{He}^+$ was not detected toward S212 and the ^4He data are of poor quality. S212 is nonetheless a potentially important object with $R_{\text{gal}} = 14.2$ kpc. The nebula is ionized by an early-type star, O5.5–O8. Optical observations measure $y_4^+ = 0.088$ –0.10; most of the helium should be ionized. We adopt $y_4^+ = 0.088$ which gives an ionization correction of $\kappa_i = 1.14$.

S228 — $^3\text{He}^+$ was not detected toward S228 and the He91 α line is only a probable detection. As is the case for S212, this outer Galaxy nebula is potentially a good ^3He candidate. Based on both radio and optical data, however, this region is ionized by a late-type O-star; the helium is probably not fully ionized within the H II region. Because $^3\text{He}^+$ and $^4\text{He}^+$ have not been detected we have a direct measure of neither the $^3\text{He}/\text{H}$ abundance nor the ionization correction.

S235, S76, S90 — These physically small, shell-like nebulae were observed because they have a morphology that is similar to that of W3A. The anomalously high $^4\text{He}/\text{H}$ abundance ratio in W3A might be caused by local enrichment from nearby, evolved objects. This might also explain the high W3 $^3\text{He}/\text{H}$ abundance ratio (Olive et al. 1995).

$^3\text{He}^+$ was not detected in either S235 or S76. Although we do not have good quality $^4\text{He}^+$ data it is clear that the helium in these nebulae is significantly under-ionized (Paper I). Both radio and optical data show that these two H II regions are ionized by late O-type or early B-type stars. Given these soft radiation fields even a high $^3\text{He}/\text{H}$ abundance ratio would be difficult to detect.

In S90, both $^3\text{He}^+$ and $^4\text{He}^+$ are detected. Although an O9.5 star is optically identified near S90, Crampton et al. (1978) argue that this star does not excite the nebula. The radio continuum data suggest an earlier type object, O8–O6.5, roughly consistent with the observed value of $y_4^+ = 0.070$. We adopt an ionization correction factor of $\kappa_i = 1.43$.

S252 — Also known as NGC 2175 or W13, this diffuse H II region extends over 25' on the sky and contains several compact components. The nebula is ionized mainly by an O6–O6.5 star centered on the H II region (Haikala 1995). Our observed position lies on a bright rim located at the western edge of the nebula (Felli et al. 1977). Because of the low emission measures in S252 there is only a probable detection of He91 α (Paper I). $^4\text{He}^+$ is, however, detected at optical wavelengths. Shaver et al. (1983) measured $y_4^+ = 0.051$ near our position. Towards the center of the H II region this value increases with $y_4^+ = 0.091$ –0.10 (Shaver et al. 1983; Deharveng et al. 2000). We adopt an ionization correction factor of $\kappa_i = 1.96$.

S311 — S311 is thought to be ionized by an O6–O6.5 star located north of the radio emission peak (Persi et al. 1987). The asymmetric density distribution suggests a blister type geometry (Albert et al. 1986). He91 α emission is detected: $y_4^+ = 0.071$. We adopt an ionization correction factor of $\kappa_i = 1.41$.

Sgr B2 — Sgr B2 is the most complex source in our sample. It is important because it is located near the Galactic Center (GC). The ionized gas is observed at high spatial resolution with radio interferometers (e.g., Martin & Downes 1972; Benson & Johnston 1984; Gaume & Claussen 1990; Gaume et al. 1995). There are at least 57 separate, compact components associated with Sgr B2 (DePree et al. 1996).

The ${}^4\text{He}^+/\text{H}^+$ abundance in Sgr B2 is known to be anomalous (see Lockman & Brown 1982, and references within). The radio continuum emission implies a very high excitation but the ${}^4\text{He}^+/\text{H}^+$ ratio is at times reported to be below 0.06 (e.g., Table 4). In the literature the Sgr B2 ${}^4\text{He}/\text{H}$ abundance is reported as underabundant, overabundant, or normal, depending on various effects such as the geometric effect, selective photo-absorption by dust, or the external maser effect. These uncertainties are compounded by complex spectral baselines produced by reflections from the telescope structure for the single-dish observations.

Some insight can, however, be gleaned from high resolution interferometric observations of RRL emission. Sgr B2 was observed with the VLA in 76 α emission (Roelfsema et al. 1987); 110 α emission (Mehringer et al. 1993); and 66 α emission (DePree et al. 1995, 1996). The ${}^4\text{He}^+/\text{H}^+$ ratio varies from 0.05 to 0.17 among the various compact components; the average value is 0.10 (Roelfsema et al. 1987; DePree et al. 1996). The component F bright cluster of sources is the sole extremely low ${}^4\text{He}^+/\text{H}^+$ ratio, $y_4^+ \leq 0.05$, component (DePree et al. 1996).

Most of the radio continuum flux density at X-band arises from the compact components towards Sgr B2 (Balsler et al. 1995). The Sgr B2 F components have the highest peak emission measures. Since the RRL emission is proportional to emission measure, the ${}^4\text{He}^+$ RRL emission is strongly influenced by the F components. It is therefore not surprising that, depending on frequency and spatial resolution, different y_4^+ values are measured in Sgr B2. Because toward Sgr B2 there is ionization structure coupled with very complex density structure within the 3'5 beam of the 140 Foot telescope, using equation (1) is inappropriate. For this source we can only adopt a limit to the ${}^3\text{He}/\text{H}$ abundance ratio.

G1.1 — Better known as Sgr D, this H II region is located only 1° from the GC but is much less complex than Sgr B2. Although we have placed its location at the GC there is evidence suggesting that it might be located outside the molecular nuclear disk (Lis 1991; Mehringer et al. 1998; Blum & Damiani 1999). High resolution radio continuum images re-

veal several compact components within a diffuse, extended halo (Liszt 1992; Mehringer et al. 1998). A single O7 star can ionize the core (Liszt 1992). This is consistent with narrow band imaging at $2.17\mu\text{m}$, $\text{Br}\gamma$, and $2.06\mu\text{m}$, and He I (Blum et al. 1999). If the diffuse gas is included in the analysis an O4 star is required to account for the excitation (Table 4). The ${}^4\text{He}^+/\text{H}^+$ ratio of 0.064 implies the presence of some neutral helium in the nebula. This is also consistent with the infrared observations of Blum et al. (1999). Initially G1.1 was classified as complex because of scant data; additional RRL data supports a simple homogeneous model. We therefore adopt the ionization correction factor of $\kappa_i = 1.56$.

M17 — The Omega nebula, also known as M17, S45, NGC 6618, and W28, is a well studied inner Galaxy H II region. The nebula spans over $10'$ in angular size and consists of two main components: M17 north (M17N) and M17 south (M17S). The Omega nebula is complex: high resolution radio continuum images reveal this density structure directly (Felli et al. 1984). We were unable to model the density structure in Paper II. The complex velocity field produces non-Gaussian profiles in both M17N and M17S (Paper I; also see Joncas & Roy 1986).

It is nonetheless clear that most of the helium is ionized. High extinction makes optical identification of the ionizing stars difficult, but infrared spectrophotometry shows at least five O3-O6 stars (Hanson & Conti 1995). The large number of early O-type stars and the high ${}^4\text{He}^+/\text{H}^+$ abundance ratios observed at both radio and optical wavelengths suggest that $\kappa_i \approx 1$. Using the He91 α transitions we adopt an ionization correction factor of $\kappa_i = 1.09$ and 1.06 for M17S and M17N, respectively.

W43 — W43 is a large, optically obscured H II region located only 4.6 kpc from the GC. Because H II regions are sparse between the GC and 4.5 kpc (Lockman et al. 1996), W43 probes the ${}^3\text{He}/\text{H}$ abundance near the outer edge of this H II region desert. W43 contains low density, diffuse gas and many compact components (e.g., Subrahmanyan & Goss 1996; Balser et al. 2001). Near infrared observations show a star cluster at the center of the H II region consisting of a WN7 star and two O-type stars (Blum et al. 1999). The total H-ionizing luminosity is considerable, requiring at least an O4 star for the entire region (Table 4).

We studied the helium ionization properties of both the diffuse and compact gas in W43 using the 140 Foot telescope and the VLA (Balser et al. 2001). Using RRL emission we imaged the ${}^4\text{He}^+/\text{H}^+$ abundance ratio for both the compact and diffuse components. The average ${}^4\text{He}^+/\text{H}^+$ ratio of the entire dataset is $\langle y_4^+ \rangle = 0.077 \pm 0.01$. We find no significant variations of the ${}^4\text{He}^+/\text{H}^+$ abundance, even for positions observed at the edge of the nebula with the 140 Foot. Thus although W43 is a complex nebula, the ionization properties do not appear to vary within this object so we can derive an accurate ionization correction factor.

We adopt $\kappa_i = 1.30$ based on the average y_4^+ abundance.

W49 — W49 is one of the most luminous H II regions in the Galaxy, consisting of a ring of ultra compact H II regions (UC H II regions), each containing at least one O-type star (e.g., Welch et al. 1987). These UC H II regions make up only one-third of the total H-ionizing luminosity observed (Conti & Blum 2002). The He91 α RRL gives a ${}^4\text{He}^+/\text{H}^+$ abundance ratio of 0.079 ± 0.0052 , consistent with the K-band data. Higher resolution VLA H and He RRL images find y_4^+ ranging from 0.05 ± 0.02 to 0.18 ± 0.06 in 13 objects with an average of $\langle y_4^+ \rangle = 0.11 \pm 0.01$ (DePree et al. 1997). This significant ionization structure combined with considerable density structure makes any equation (1) type ionization correction inappropriate. We therefore adopt $\kappa_i \geq 1$.

W51 — W51 is a bright, complex H II region with an angular extent of 2° on the sky. Radio continuum observations reveal several O4–O6 stars associated with the main components (Mehringer 1994). Mid-infrared imaging and spectroscopy suggests stars with spectral types \sim O9 (Okamoto et al. 2001). The X-band ${}^4\text{He}^+$ RRL data give a y_4^+ abundance of 0.079 ± 0.0024 . The He70 α transition appears to be slightly lower with $y_4^+ \sim 0.07$. High resolution VLA observations of 92 α RRLs yield y_4^+ values ranging from 0.08 ± 0.02 to 0.14 ± 0.06 with an average of $\langle y_4^+ \rangle = 0.096 \pm 0.015$ (Mehringer 1994). Although most of the helium appears to be ionized, given the complexity of this object we adopt an ionization correction factor of $\kappa_i \geq 1$.

S156 — S156 is a compact H II region excited by an O6.5-type star. We have only an upper limit for the ${}^3\text{He}^+/\text{H}^+$ abundance. Although we have detected ${}^4\text{He}^+$ at X-band the accuracy is not very good. Optical observations yield $y_4^+ = 0.081$ (Deharveng et al. 2000). We adopt an ionization correction factor of $\kappa_i = 1.23$.

NGC 7538 — Also known as S158, NGC 7538 is centrally diffuse with a bright rim to the west (Israel 1977). An O7 star located at the center of the nebula is responsible for the excitation (Deharveng et al. 1979). Optical data yield $y_4^+ = 0.10$ (Lynds & O’Neil, Jr. 1986), a value higher than our RRL results. Both the X-band and K-band data give $y_4^+ \sim 0.08$, although the He114 β transition produces a slightly higher value of 0.10. We adopt an ionization correction factor based on the X-band data of $\kappa_i = 1.19$.

S162 — Sometimes called the Bubble nebula, S162 consists of a circularly shaped shell with bright emission to the north observed in H α and the radio continuum (Barlow et al. 1976; Israel et al. 1973, Paper I). The exciting star has been classified as an O6.5-type, consistent with the radio continuum estimates. We do not detect ${}^3\text{He}^+$ emission. Although we do detect the He91 α RRL, the quality factor is poor. We cannot make an ionization correction so therefore adopt $\kappa_i \geq 1$.

5. DISCUSSION

Our nebular ionization correction, κ_i , is the simplest possible approach to the problem. It makes several key assumptions: (1) the ${}^4\text{He}$ abundance is ${}^4\text{He}/\text{H} \equiv 0.10$ for all Galactic H II regions; (2) all the He is singly ionized—there is neither neutral nor doubly ionized He within the nebulae; and (3) the ${}^3\text{He}^+$ and ${}^4\text{He}^+$ ions occupy identical volumes within the nebulae. Measuring the total helium abundance is difficult since there is no direct way to observe neutral helium. We do not expect any significant doubly ionized helium since the radiation field from Galactic O-type stars is not hard enough. For example, M17 is ionized by several stars classified between O3–O6 (Hanson & Conti 1995) and is one of the Galactic H II regions with the highest degree of ionization. Yet only a very low upper limit, ${}^3\text{He}^{++}/\text{H}^+ < 8 \times 10^{-5}$, is measured for ${}^4\text{He}^{++}$ in M17 (Peimbert et al. 1992b). In fact, to our knowledge ${}^4\text{He}^{++}$ has never been detected in any Galactic H II region.

A canonical value for the Galactic ${}^4\text{He}$ abundance of $y_4 = 0.1$ is typically used in the literature. Most of the ${}^4\text{He}$ was produced during the era of primordial nucleosynthesis. Therefore the variation of ${}^4\text{He}$ in the Galaxy, caused by stellar and Galactic evolution, is expected to be small because $\Delta Y/\Delta Z \sim 1$, where Y and Z are the helium and metal abundances by mass (e.g., Chiappini et al. 2002). Direct measurement of the total ${}^4\text{He}/\text{H}$ abundance ratio in the Galaxy is difficult. The ${}^4\text{He}$ abundance cannot be determined using either the Solar photosphere or in meteorites. Measurements of ${}^4\text{He}$ in Galactic H II regions have to correct for ionization structure just as we are trying to do here for ${}^3\text{He}$.

Solar ${}^4\text{He}$ abundances are determined from theoretical stellar evolution models with $y_4 \sim 0.1$ (e.g., Anders & Grevesse 1989). Peimbert (1993) suggested that the high excitation H II region M17 was the best object to measure ${}^4\text{He}$ directly and they also determined $y_4 \sim 0.1$. There is mounting evidence, however, that y_4 is less than 0.1 in the Galaxy. More recent calibration of the ${}^4\text{He}$ Solar abundances yield y_4 values lower by as much as 10% (Grevesse et al. 1996, 1998; Basu & Anita 2004; Asplund et al. 2005). Recent estimates of y_4 in M17 that include temperature fluctuations reduce y_4 by about 5%, consistent with improved RRL data (Peimbert & Peimbert 2002; Quireza et al. 2006a). Furthermore, RRL observations of the lower metallicity Galactic H II region S206, which is also expected to contain little or no neutral helium, give $y_4 = 0.085$ (Balsler 2006).

Nevertheless, we adopt $y_4 \equiv y_{4\text{GAL}} = 0.1$ in equation (1) for our ionization correction factor analysis. We judge that for our simple sources the ionization correction should be good to about 10%. At this level of accuracy all of the additional ionization effects considered by ${}^4\text{He}$ abundance analyses (e.g., Izotov et al. 2007) can be neglected.

6. SUMMARY

The significance of our results for both primordial ${}^3\text{He}$ and chemical evolution of ${}^3\text{He}$ lies in the fact that the abundances we find are quite low. Hence we have paid particular attention to factors that might lead us to measure a lower abundance than that which is actually present. In this paper we conclude that it is unlikely that large ionization corrections are required for our high excitation state ${}^3\text{He}$ nebulae. We use the y_4^+ abundance to select for high excitation H II regions. We determined an ionization correction factor for the Paper I nebular sample. There would have to be a conspiracy between the density and ionization structure for these ionization corrections to be underestimated by a substantial amount. Our synthetic nebular models (§3) do show that large ionization corrections are possible. Such models, however, require that there be rather specific density and ionization structure configurations. Our simple ionization correction fails when y_4^+ changes significantly between the low density gas where ${}^3\text{He}^+$ dominates the emission and the high density gas where ${}^4\text{He}^+$ dominates. The more complex the source the larger our potential error in determining the ionization correction. We find both numerically and observationally that the simple sources give the best ionization corrections (§4).

For the sources that we classify as simple and which also have well determined line parameters, the ionization correction given in §4 should be accurate. Indeed, the major uncertainty is likely to be the value adopted for $y_{4\text{GAL}}$. Even for more complex sources our simple ionization correction should be reasonable for any nebula that does not have large fluctuations in excitation. We have shown this to be the case for the complex nebula W43 where we have single-dish and interferometry data for both radio recombination line and continuum emission (§4).

For a subset of our ${}^3\text{He}$ sources, we use both 8 GHz and 18 GHz RRL data to derive y_4^+ . The two sets of observations probe different regions of the nebula, yet we in general find very similar values for y_4^+ . This is consistent with the notion that for our sources selected for high excitation there are not large ionization corrections.

We can use this simple ionization correction analysis because unlike many of the light elements ${}^3\text{He}/\text{H}$ abundances accurate to $\sim 10\%$ can yield important conclusions for both the primordial ${}^3\text{He}$ and the chemical evolution of ${}^3\text{He}$ (Wilson & Rood 1994). This is in stark contrast to the situation for ${}^4\text{He}$ where the ${}^4\text{He}/\text{H}$ abundance needs to be determined to an accuracy of $\lesssim 1\%$ if one is to draw cosmologically significant inferences (e.g., Izotov et al. 2007). Furthermore, because the majority of our ${}^3\text{He}$ nebulae are not optically visible it is not likely that we will ever have sufficiently detailed information about their physical properties to make a significantly better correction.

We thank the staff of NRAO Green Bank for their help, support, and friendship. The ^3He research has been sporadically supported by the National Science Foundation (AST 97-31484; AST 00-98047; AST 00-98449). This research has made use of NASA's Astrophysics Data System and the SIMBAD database, operated at CDS, Strasbourg, France.

REFERENCES

- Adler, D. S., Wood, D. O. S., & Goss, W. M. 1996, *ApJ*, 471, 871
- Albert, C. E., Schwartz, P. R., Bowers, P. F., & Rickard, L. J. 1986, *AJ*, 92, 75
- Anders, E., & Grevesse, N. 1989, *Geochim. Cosmochim. Acta*, 53, 197
- Armour, M., Ballantyne, D. R., Ferland, G. J., Karr, J., & Marin, P. G. 1999, *PASP*, 111, 1251
- Asplund, M., Grevesse, N., & Sauval, A. J. 2005, in *ASP Conf. Ser. 336, Cosmic Abundances as Records of Stellar Evolution and Nucleosynthesis*, ed. T. G. Barnes III & F. N. Bash (San Francisco: ASP) 25
- Baldwin, J. A., Ferland, G. J., Martin, P. G., Corbin, M. R., Cota, S. A., Peterson, B. M., & Slettebak, A. 1991, *ApJ*, 374, 580
- Ballantyne, D. R., Ferland, G. J., & Martin, P. G. 2000, *ApJ*, 536, 773
- Balser, D. S. 1995, PhD dissertation, Boston University
- Balser, D. S. 2006, *AJ*, 132, 2326
- Balser, D. S., Bania, T. M., Brockway, C. J., Rood, R. T., & Wilson, T. L. 1994, *ApJ*, 430, 667
- Balser, D. S., Bania, T. M., Rood, R. T., & Wilson, T. L. 1995, *ApJS*, 100, 371
- Balser, D. S., Bania, T. M., Rood, R. T., & Wilson, T. L. 1997, *ApJ*, 483, 320
- Balser, D. S., Bania, T. M., Rood, R. T., & Wilson, T. L. 1999, *ApJ*, 510, 759 (Paper II)
- Balser, D. S., Goss, W. M., Bania, T. M., & Rood, R. T. 2006, *ApJ*, 640, 360
- Balser, D. S., Goss, W. M., & De Pree, C. G. 2001, *ApJ*, 121, 371

- Bania, T. M., Balser, D. S., Rood, R. T., Wilson, T. L., & Wilson, T. J. 1997, *ApJS*, 113, 353 (Paper I)
- Bania, T. M., Rood, R. T., & Balser, D. S. 2002, *Nature*, 415, 54
- Barlow, M. J., Cohen, M., Gull, T. R. 1976, *MNRAS*, 176, 359
- Benson, J. M., & Johnston, K. J. 1984, *ApJ*, 277, 181
- Basu, S., & Anita, H. M. 2004, *ApJ*, 606, L85
- Blagrove, K. P. M., Martin, P. G., Rubin, R. J., Dufour, R. J., Baldwin, J. A., Hester, J. J., & Walter, D. K. 2007, *ApJ*, 655, 299
- Blum, R. D., & Daminieli, A. 1999, *ApJ*, 512, 237
- Blum, R. D., Daminieli, A., & Conti, P. S. 1999, *AJ*, 117, 1392
- Caplan, J., Deharveng, L., Peña, M., Costero, R., & Blondel, C. 2000, *MNRAS*, 311, 317
- Carpenter, J. M., Heyer, M. H., & Snell, R. L. 2000, *ApJS*, 130, 381
- Charbonnel, C. 1998, *Space Science Reviews*, 84, 199
- Chiappini, C., Renda, A., & Matteucci, F. 2002, *A&A*, 395, 789
- Chini, R., & Wink, J. E. 1984, *A&A*, 139, L5
- Conti, P. S., & Alschuler, W. R. 1971, *ApJ*, 170, 325
- Conti, P. S., & Leep, E. M. 1974, *ApJ*, 193, 113
- Conti, P. S., & Blum, R. D. 2002, *ApJ*, 564, 827
- Crampton, D. 1971, *AJ*, 76, 260
- Crampton, D., Georgelin, Y. M., & Georgelin, Y. P. 1978, *A&A*, 66, 1
- Deharveng, L., Lortet, M. C., & Testor, G. 1979, *A&A*, 71, 151
- Deharveng, L., Peña, M., Caplan, J., & Costero, R. 2000, *MNRAS*, 311, 329
- De Pree, C. G., Gaume, R. A., Goss, W. M., & Claussen, M. J. 1995, *ApJ*, 451, 284
- De Pree, C. G., Gaume, R. A., Goss, W. M., & Claussen, M. J. 1996, *ApJ*, 464, 788
- De Pree, C. G., Mehringer, D. M., Goss, W. M. 1997, *ApJ*, 482, 307

- Esteban, C., Peimbert, M., Torres-Peimbert, S., & Escalante, V. 1998, MNRAS, 295, 401
- Esteban, C., Peimbert, M., Torres-Peimbert, S., & García-Rojas 1999, Rev. Mexicana de Astron. y Astrofis., 35, 65
- Feinstein, A. & Vázquez, R. A. 1989, A&AS, 77, 321
- Felli, M., Habing, H. J., & Israel, F. P. 1977, A&A, 59, 43
- Felli, M., Massi, M., & Churchwell, E. 1984, A&A, 136, 53
- Fich, M., & Silkey, M. 1991, ApJ, 366, 107
- Gaume, R. A., & Claussen, M. J. 1990, ApJ, 351, 538
- Gaume, R. A., Claussen, M. J., De Pree, C. G., Goss, W. M., & Mehringer, D. M. 1995, ApJ, 449, 663
- Georgelin, Y. M. 1975, Thèse d'État, Univ. de Provence (Univ. d'Aix-Marseille I)
- Georgelin, Y. M., Georgelin, Y. P., & Roux, S. 1973, A&A, 25, 337
- Grevesse, N., Noels, A., & Sauval, A. J. 1996, in ASP Conf. Ser. 99, Cosmic Abundances, ed. S. S. Holt & G. Sonneborn (San Francisco: ASP), 117
- Grevesse, N., Sauval, A. J. 1998, Space Sci. Rev., 85, 161
- Gruenwald, R., Steigman, G., & Viegas, S. M 2002, ApJ, 567, 931
- Goy, G. 1980, A&AS, 1980, 42, 91
- Gulyaev, S. A., Sorochenko R. L., & Tsivilev, A. P. 1997, Astronomy Letters, 23, 165
- Haikala, L. K. 1995, A&A, 294, 89
- Hanson, M. M., & Conti, P. S. 1995, ApJ, 448, L45
- Hunter, D. A., & Massey, P. 1990, AJ, 99, 846
- Israel, F. P. 1977, A&A, 59, 27
- Israel, F. P., Habing, H. J., & de Jong, T. 1973, A&A, 27, 143
- Izotoz, Y. I., Thuan, T. X., & Stasińska, G. 2007, astro-ph/0702072
- Joncas, G., & Roy, J.-R. 1986, ApJ, 307, 649

- Lockman, F. J., & Brown, R. L. 1982, *ApJ*, 259, 595
- Lockman, F. J., Pisano, D. J., & Howard, G. J. 1996, *ApJ*, 472, 173
- Lis, D. C. 1991, *ApJ*, 379, L53
- Liszt, H. S. 1992, *ApJS*, 82, 495
- Lynds, B. T., & O’Neil Jr., E. J. 1986, *ApJ*, 306, 532
- Martin, A. H. M., & Downes, D. 1972, *Astrophysical Letters*, 11, 219
- Mathis, J. S. 1982, *ApJ*, 261, 195
- Mathis, J. S. 1985, *ApJ*, 291, 247
- Mathis, J. S., & Rosa, M. R. 1991, *A&A*, 245, 625
- Mathis, J. S., & Wood, K. 2005, *MNRAS*, 360, 227
- Mehring, D. M. 1994, *ApJS*, 91, 713
- Mehring, D. M., Palmer, P., Goss, W. M., & Yusef-Zadeh, F. 1993, *ApJ*, 412, 684
- Mehring, D. M., Goss, W. M., Lis, D. C., Palmer, P., & Menten, K. M. 1998, *ApJ*, 493, 274
- Miller, J. S., 1968, *ApJ*, 151, 473
- Moffat, A. F. J., Fitzgerald, M. P., & Jackson, P. D. 1979, *A&AS*, 38, 197
- Moreno, M. A., & Chavarría-K., C. 1986, *A&A*, 161, 130
- Okamoto, Y. K., Kataza, H., Yamashita, T., Miyata, T., & Onaka, T. 2001, *ApJ*, 553, 254
- Olive, K. A., Rood, R. T., Schramm, D. N., Truran, J., & Vangioni-Flam, E. 1995, *ApJ*, 444, 680
- Panagia, N. 1973, *AJ*, 78, 929
- Peimbert, M. 1993, *Rev. Mexicana Astron. Astrofis.*, 27, 9
- Peimbert, M., & Peimbert, A. 2002, *Rev. Mexicana Astron. Astrofis. Ser. Conf.*, 14, 47
- Peimbert, A., Peimbert, M. & Luridiana, V. 2002, *ApJ*, 565, 668

- Peimbert, M., Rodríguez, L. F., Bania, T. M., Rood, R. T., & Wilson, T. L. 1992a, *ApJ*, 395, 484
- Peimbert, M., Torres-Piembert, S., & Ruiz, M. T. 1992b, *Rev. Mexicana Astron. Astrofis.*, 24, 155
- Peng, B., Kraus, A., Krichbaum, T. P., & Witzel, A. 2000, *A&AS*, 145, 1
- Persi, P., Ferrari-Toniolo, Shivanandan, K., & Spinoglio, L. 1987, *A&AS*, 70, 437
- Pogge, R. W., Owen, J. M., & Atwood, B. 1992, *ApJ*, 399, 147
- Quireza, C., Rood, R. T., Balser, D. S., & Bania, T. M., 2006a, *ApJS*, 165, 338
- Quireza, C., Rood, R. T., Bania, T. M., Balser, D. S. & Maciel, W. J., 2006b, 653, 1226
- Roelfsema, P. R., Goss, W. M., Whiteoak, J. B., Gardner, F. F., & Pankonin, V. 1987, *A&A*, 175, 219
- Roelfsema, P. R., & Goss, W. M. 1991, *A&AS*, 87, 177
- Roelfsema, P. R., Goss, W. M., & Mallik, D. C. V. 1992, *ApJ*, 394, 188
- Romano, D., Tosi, M., Matteucci, F., & Chiappini, C. 2003, *MNRAS*, 346, 295
- Rood, R. T., Bania, T. M., Balser, D. S., & Wilson, T. L. 2007, *ApJ*, in preparation (Paper IV)
- Rubin, R. H. 1984, *ApJ*, 287, 653
- Rubin, R. H., Simpson, J. P., Haas, M. R., Erickson, E. F. 1991, *ApJ*, 374, 564
- Sauer, D., & Jedamzik, K. 2002, *A&A*, 381, 361
- Schraml, J., & Mezger, P. G. 1969, *ApJ*, 156, 269
- Shaver, P. A., McGee, R. X., Newton, L. M., Danks, A. C., & Pottasch, S. R. 1983, *MNRAS*, 204, 53
- Shields, G. A., & Searle, L. 1978, *ApJ*, 222, 821
- Subrahmanyan, R. & Goss, W. M. 1996, *MNRAS*, 281, 239
- Thronson, Jr., H. A., Schwartz, P. R., Smith, H. A., Lada, C. J., Glaccum, W., Harper, D. A. 1984, *ApJ*, 284, 597

- Vacca, W. D., Garmany, C. D., & Shull, J. M. 1996, *ApJ*, 460, 914
- Viegas, S. M., Gruenwald, R., & Steigman, G. 2000, *ApJ*, 531, 813
- Vílchez, J. M., & Esteban, C. 1996, *MNRAS*, 280, 720
- Vílchez, J. M., & Pagel, B. E. J. 1988, *MNRAS*, 231, 257
- Wilson, T. L., & Rood, R. T. 1994, *ARA&A*, 32, 191
- Welch, W. J., Dreher, J. M., Jackson, J. M., Terebey, S., & Vogel, S. N. 1987, *Science*, 238, 1550
- Yang, J., Turner, M. S., Steigman, G., Schramm, D. N., & Olive, K. A. 1984, *ApJ*, 281, 493

Table 1. K-band (18 GHz) Radio Recombination Line Parameters

Source	Transition	T_L (mK)	$\sigma(T_L)$ (mK)	Δv (km s ⁻¹)	$\sigma(\Delta v)$ (km s ⁻¹)	t_{intg} (hr)	RMS (mK)	Quality Factor
W3.....	H70 α	579.63	0.76	27.44	0.04	11.4	0.97	A
	He70 α	60.85	0.88	20.94	0.36	11.4	0.97	B
	H88 β	160.73	0.31	27.80	0.06	13.0	0.61	A
	He88 β	17.30	0.36	21.21	0.53	13.0	0.61	B
G133.8.....	H70 α	64.99	0.47	30.06	0.25	23.6	0.48	B
	He70 α	6.04	0.55	22.94	2.56	23.6	0.48	C
	H88 β	19.63	0.24	30.14	0.42	22.2	0.51	C
	He88 β	1.41	0.36	13.01	4.05	22.2	0.51	D
S206.....	H70 α	29.24	0.15	27.32	0.16	26.0	0.50	B
	He70 α	3.19	0.16	21.89	1.33	26.0	0.50	C
	H88 β	8.29	0.10	26.61	0.38	26.0	0.43	C
S209.....	H70 α	22.24	0.15	29.70	0.23	30.8	0.39	B
	He70 α	1.74	0.17	23.07	2.71	30.8	0.39	D
	H88 β	7.20	0.14	29.22	0.67	30.4	0.41	C
M17N.....	H70 α	387.81	3.28	33.11	0.32	8.0	1.97	A
	He70 α	39.74	3.60	27.69	2.94	8.0	1.97	B
	H88 β	111.53	1.04	33.27	0.36	8.0	0.89	A
	He88 β	11.93	1.21	25.32	3.16	8.0	0.89	B
M17S.....	H70 α	835.20	5.25	35.29	0.26	4.8	2.16	A
	He70 α	77.02	5.41	34.25	2.98	4.8	2.16	B
	H88 β	245.60	1.46	35.91	0.25	4.8	1.57	A
	He88 β	22.27	1.51	34.97	2.96	4.8	1.57	B
W43.....	H70 α	241.82	0.45	33.34	0.07	21.0	0.94	A
	He70 α	19.37	0.47	31.37	0.98	21.0	0.94	B
	H88 β	71.83	0.19	32.55	0.10	21.0	0.73	A
	He88 β	6.34	0.21	26.81	1.09	21.0	0.73	C
W49.....	H70 α	417.38	0.60	29.69	0.05	20.2	0.85	A
	He70 α	41.31	0.69	23.94	0.65	20.2	0.85	B
	H88 β	107.21	0.28	29.55	0.09	20.2	0.76	A
	He88 β	10.67	0.34	21.55	1.29	20.2	0.76	B

Table 1—Continued

Source	Transition	T_L (mK)	$\sigma(T_L)$ (mK)	Δv (km s ⁻¹)	$\sigma(\Delta v)$ (km s ⁻¹)	t_{intg} (hr)	RMS (mK)	Quality Factor
W51.....	H70 α	971.22	0.58	29.53	0.02	8.4	2.80	A
	He70 α	87.97	0.66	23.44	0.21	8.4	2.80	A
	H88 β	248.53	0.32	29.77	0.04	8.4	1.15	A
	He88 β	23.75	0.36	25.65	0.86	8.4	1.15	B
NGC7538.....	H70 α	126.41	0.23	27.59	0.06	25.2	0.52	A
	He70 α	13.17	0.26	21.90	0.53	25.2	0.52	B
	H88 β	37.87	0.14	28.22	0.12	24.4	0.45	B
	He88 β	3.49	0.17	20.59	1.35	24.4	0.45	C

Table 2. NEBULA Model Parameters^a

Model	Component 1					Component 2				
	θ_s ($'$)	n_e (cm^{-3})	M_f	y_3^+ (10^{-5})	y_4^+	θ_s ($'$)	n_e (cm^{-3})	M_f	y_3^+ (10^{-5})	y_4^+
A1	3.5	100	1.00	1.0	0.10
A2	3.5	100	1.00	0.7	0.07
B	1.5	500	0.30	1.0	0.10	3.5	100	0.70	1.0	0.10
C	1.5	100	0.08	1.0	0.10	3.5	100	0.92	0.5	0.05
D	1.5	100	0.08	0.5	0.05	3.5	100	0.92	1.0	0.10
E	1.5	500	0.30	1.0	0.10	3.5	100	0.70	0.5	0.05
F	1.5	500	0.30	0.5	0.05	3.5	100	0.70	1.0	0.10

^aThe distance to all model nebulae is 8 kpc.

Table 3. NEBULA Model Results

Model	X-band ^a						K-band ^b
	T_C (K)	T_L (mK)	y_3^+ (10^{-5})	y_4^+	κ_i	y_3 (10^{-5})	y_4^+
A1	0.93	1.10	1.00	0.100	1.00	1.00	0.100
A2	0.93	0.81	0.72	0.070	1.43	1.03	0.070
B	3.00	1.50	0.77	0.100	1.00	0.77	0.100
C	0.93	0.64	0.57	0.055	1.82	1.04	0.067
D	0.93	1.10	0.96	0.095	1.05	1.01	0.082
E	3.00	1.10	0.53	0.085	1.18	0.62	0.096
F	3.00	1.30	0.65	0.064	1.56	1.01	0.053

^a $\nu = 8$ GHz; HPBW = 3'5.

^b $\nu = 18$ GHz; HPBW = 1'5.

Table 4. H II Region Excitation Properties

Source	Radio ^a			Optical ^b	
	${}^4\text{He}^+/\text{H}^+$	N_L (s^{-1})	Spectral Type	${}^4\text{He}^+/\text{H}^+$	Spectral Type
W3	0.076 ± 0.0033	49.28	O6.5 (O5.5)
G133.8	0.082 ± 0.0075	48.96	O7.5 (O6)
S206	0.092 ± 0.0029	48.95	O7.5 (O6.5)	0.10	O4–O6
...	(8)	(7,8,13,17,20)
S209	0.083 ± 0.0037	49.82	O3 (O4)	0.084–0.12	O9
...	(8,25)	(3)
S212	...	48.67	O8.5 (O7)	0.088–0.10	O5.5–O7
...	(8,11,25)	(3,17,20)
S228	...	47.95	B0.5 (O9.5)	...	O8–B0
...	(3,17)
S235	...	47.86	B0.5 (O9.5)	...	O9.5–B0
...	(13,17)
S252	...	48.67	O8.5 (O7)	0.051	O6–O6.5
...	(24)	(5,12,14,15,19)
S311	0.071 ± 0.0038	48.93	O8 (O6.5)	...	O6–O6.5
...	(6,10,14,23)
Sgr B2	0.059 ± 0.0182	50.57	< O3 (< O4)
G1.1	0.064 ± 0.0066	49.91	O3 (O4)
M17S	0.092 ± 0.0110	50.46	< O3 (< O4)	...	O3–O6
...	(16)
M17N	0.094 ± 0.0089	49.75	O4 (O5)	0.10	O3–O6
...	(9,22)	(16)
W43	0.068 ± 0.0052	50.42	< O3 (< O4)	...	WN7
...	(2)
S76	...	47.76	> B0.5 (O9.5)
W49	0.079 ± 0.0052	50.87	< O3 (< O4)
W51	0.079 ± 0.0024	50.47	< O3 (< O4)
S90	0.070 ± 0.0067	48.87	O8 (O6.5)	...	O9.5
...	(13,14)

Table 4—Continued

Source	Radio ^a			Optical ^b	
	⁴ He ⁺ /H ⁺	N_L (s ⁻¹)	Spectral Type	⁴ He ⁺ /H ⁺	Spectral Type
S156	...	48.91	O8 (O6.5)	0.081	O6.5–O7
...	(8)	(1,12,17)
NGC 7538	0.084 ± 0.0034	49.25	O6.5 (O5.5)	0.10	O7
...	(18)	(13,21)
S162	...	48.79	O8 (O6.5)	...	O6.5
...	(4)

^aBased on the Paper I X-band radio data that are appropriate for the ³He⁺ ionization correction. The ⁴He⁺/H⁺ abundance ratio is determined using the H91α and He91α RRLs (only quality factors A and B are considered). The H-ionizing luminosity, N_L , is calculated from the radio continuum emission. The spectral type is determined from N_L and a single star ZAMS model (Vacca et al. 1996; Panagia 1973, in parentheses).

^bBased on optical data from the literature. The references are listed in parentheses.

References. — (1) Barlow et al. (1976); (2) Blum et al. (1999); (3) Chini & Wink (1984); (4) Conti & Alschuler (1971); (5) Conti & Leep (1974); (6) Crampton (1971); (7) Crampton et al. (1978); (8) Deharveng et al. (2000); (9) Esteban et al. (1999); (10) Feinstein & Vázquez (1989); (11) Fich & Silkey (1991); (12) Georgelin (1975); (13) Georgelin et al. (1973); (14) Goy (1980); (15) Haikala (1995) (16) Hanson & Conti (1995); (17) Hunter & Massey (1990); (18) Lynds & O’Neil Jr. (1986); (19) Miller (1968); (20) Moffat et al. (1979); (21) Moreno & Charvarría-K. (1986) (22) Peimbert et al. (1992b); (23) Persi et al. (1987); (24) Shaver et al. (1983); (25) Vílchez & Esteban (1996).

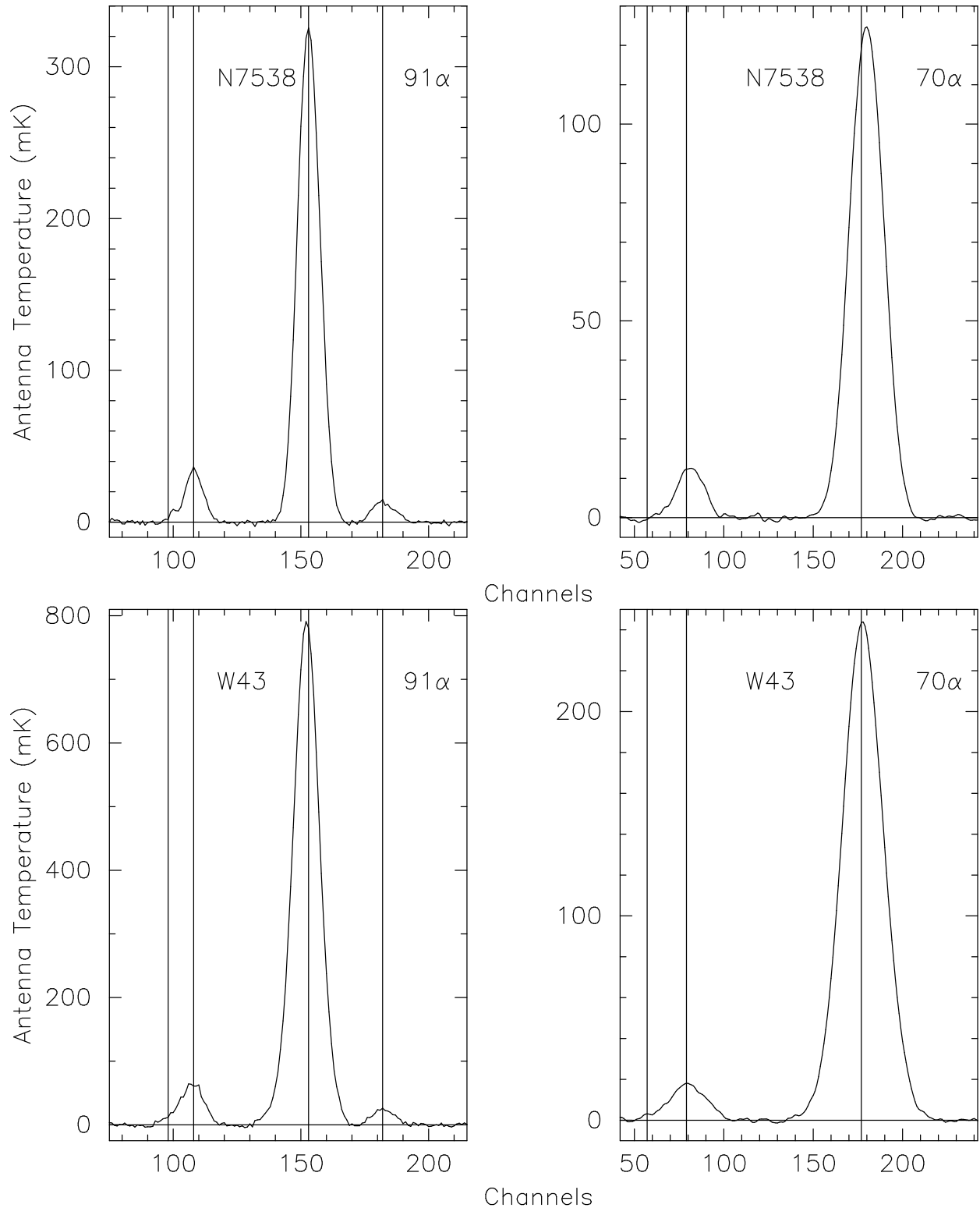


Fig. 1.— Spectra of the 91 α X-band (8 GHz) and the 70 α K-band (18 GHz) radio recombination line emission for the H II regions NGC 7538 and W43. The vertical lines flag from left to right the C, He, and H transitions. (The additional flag in the 91 α spectra is the H 154 ϵ transition.) The intensity scale is in units of milliKelvins. The LSR velocity increases from left to right at 1.3 km sec⁻¹ per channel.

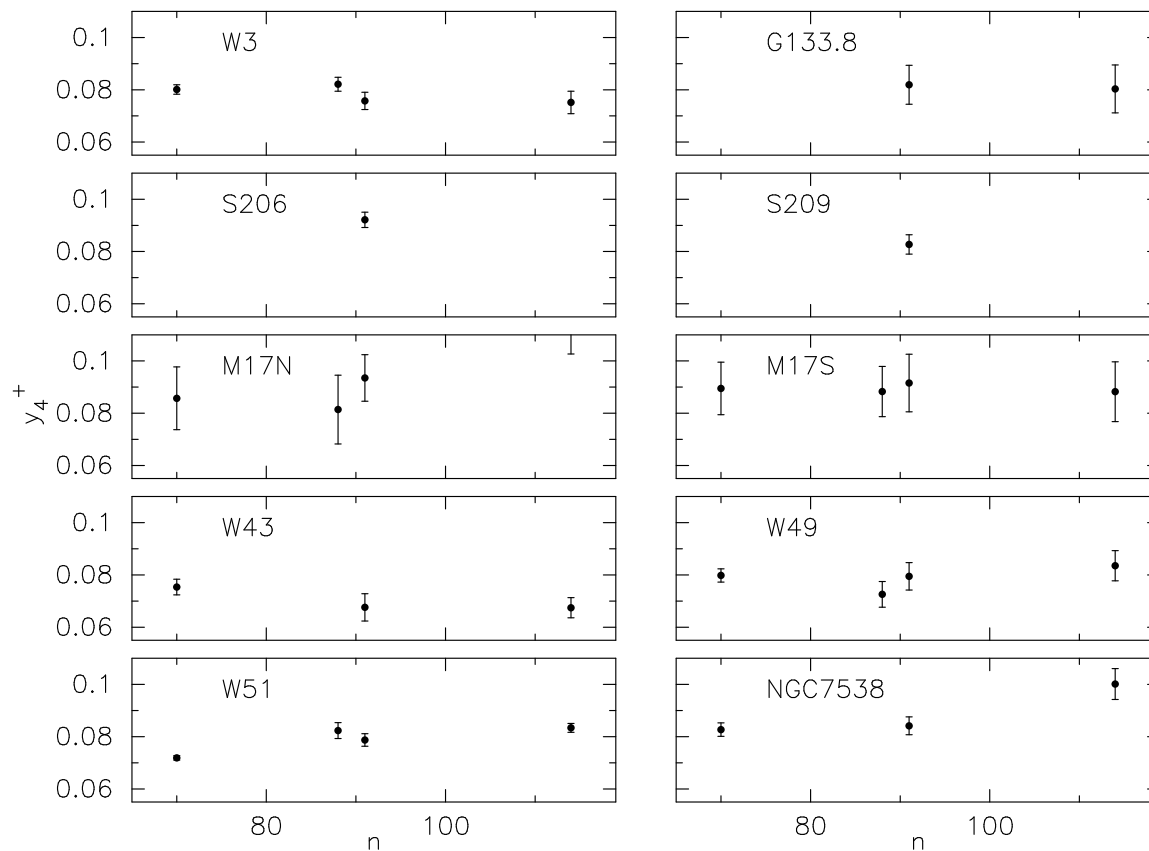


Fig. 2.— The ${}^4\text{He}^+/\text{H}^+$, y_4^+ , abundance ratio plotted as a function of the principal quantum number, n , of the RRL transition. The 70α , 88β , 91α , and 114β transitions are shown. Abundances are plotted only for transitions that have a quality factor of A or B (see Table I and Paper I).

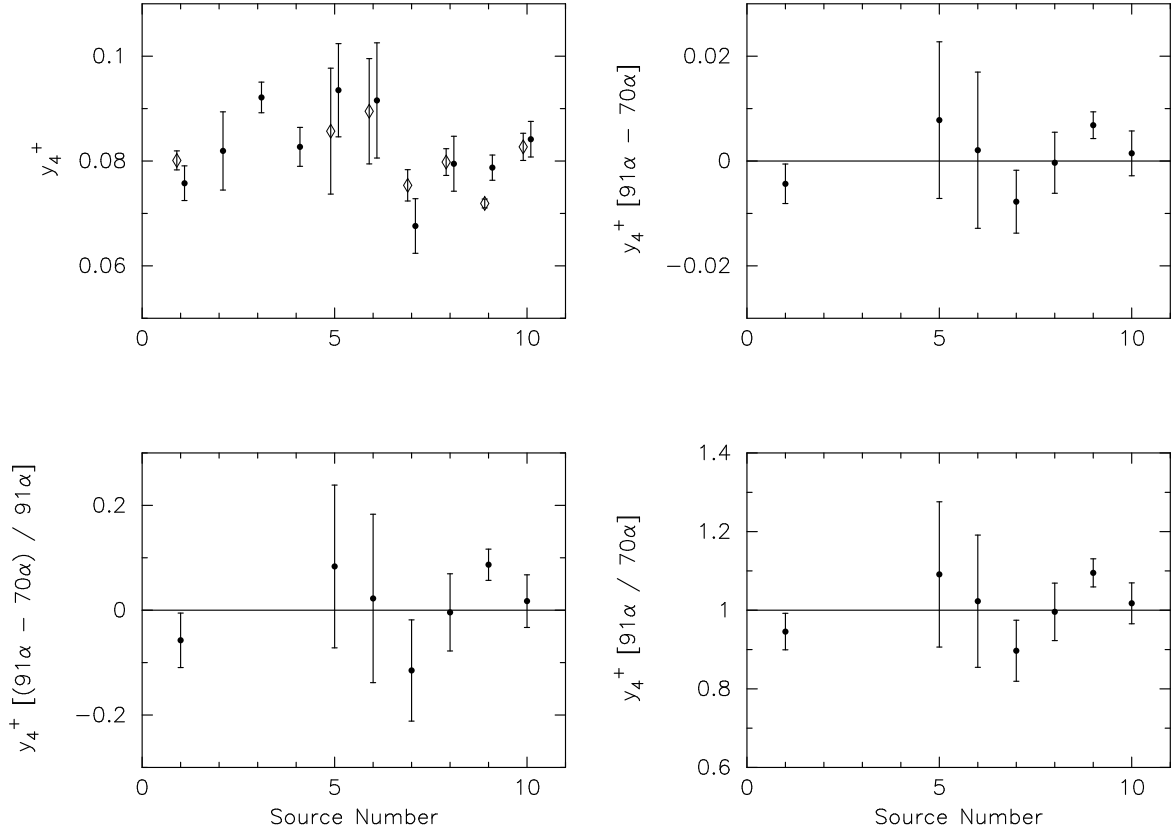


Fig. 3.— Comparison of the y_4^+ ratios derived from the H91 α and H70 α spectra for the 10 K-band sources in the order listed in Table 1. Only abundances for quality factor A or B are plotted. *Top Left:* The H91 α (circles) and H70 α (diamonds) y_4^+ ratios for each nebula. *Top Right:* The y_4^+ (H91 α) – y_4^+ (H70 α) difference. *Bottom Left:* The fractional y_4^+ deviation: $(y_4^+ (\text{H91}\alpha) - y_4^+ (\text{H70}\alpha)) / y_4^+ (\text{H91}\alpha)$. *Bottom Right:* The $y_4^+ (\text{H91}\alpha) / y_4^+ (\text{H70}\alpha)$ ratio.

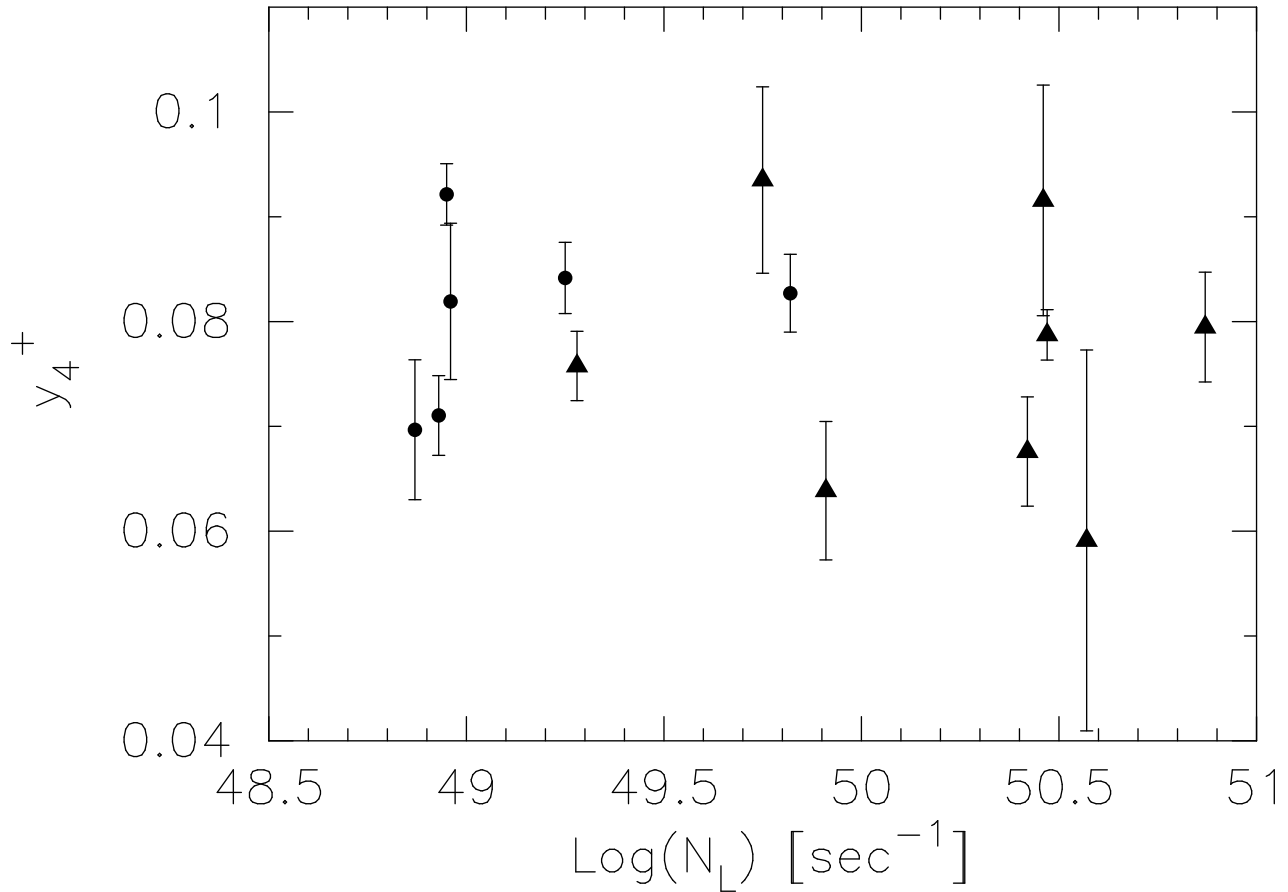


Fig. 4.— The ${}^4\text{He}^+/\text{H}^+$, y_4^+ , abundance ratio plotted as a function of the H-ionizing luminosity, N_L . The y_4^+ values are calculated using only the H91 α and He91 α transitions. Only transitions that have a quality factor of A or B (see Paper I) are shown. Circles denote simple sources; triangles identify complex sources (see text).